Parameter Sensitivity Analysis

To assess the robustness of our simulation results against numerical and algorithmic parameters, we performed a sensitivity analysis using the baseline case (release altitude 180 km, mass 10 kg, initial ionization rate 20%, at 300 s after release). Four controlling factors were examined: ray density (elevation-angle sampling step: π/2048, π/4096, and π/8192 rad), ray integration step size (0.01 km, 0.05 km, and 0.10 km), receiver acceptance radius (±0.5 km, ±1 km, and ±2 km), and cloud spatial grid spacing (0.5 km and 1 km). The detailed quantitative results are provided in Table S1.

Table S1. Sensitivity Test of Calculation Results under Different Ray Density, Integration Step Size, Receiver Range and Cloud Cluster Grid Step Sizes

Controlled variable	Parameter value	N_e_max ($\times 10^{13}$ m^{-3})	Cloud scale (km)	Shadow-zone width (km)	Enhancement-zone width (km)	Multipath delay spread (km)
Baseline[1]	π/4096; 0.05 km; ±1 km; 1 km			164	104	181.8
Ray density[2] (elevation sampling step)	Pi/2048			172	114	162.8
	Pi/8192			166	108	186.1
receiver-bin size[2]	±0.5km	1.795	34.88	169	101	90.6
	±2km			172	108	240.8
Ray integration step[2]	0.01km			164	104	172.2
	0.1km			166	104	184.3
spatial grid spacing	0.5 km	1.745	35.20	170	108	179.8

[1] For the baseline case (release altitude 180 km, mass 10 kg, initial ionization rate 20%, at 300 s after release), the sampling step angle corresponding to the ray density is pi/4096; the ray integration step length is 0.05 km; the receiver-bin size is ±1 km; and the spatial grid step of the cloud is 1 km.

[2] For the ray density, integration step, and receiver-bin size tests, the cloud evolution parameters (N_e_max and cloud scale) remain unchanged as they are independent of the ray-tracing settings.

For the baseline configuration (π/4096 rad angular step, 0.05 km integration step, ±1 km acceptance radius, and 1 km grid spacing), the peak electron density is 1.795×10^{13} m^{-3}, the cloud scale (defined as the 1/e width of the density contour) is 34.88 km, the shadow-zone width is 164 km, the enhancement-zone width is 104 km, and the multipath delay spread is 181.8 km.

Varying the ray density between π/2048 and π/8192 rad changes the shadow-zone width by no more than 5% (range 164–172 km) and the enhancement-zone width by less than 10% (104–114 km), indicating that the adopted angular step of π/4096 rad is sufficient for resolving the ground signal distribution. The ray-tracing results under different elevation sampling step sizes were shown in Figure S1. The receiver acceptance radius shows a more noticeable

effect on multipath delay spread: increasing the radius from ±0.5 km to ±2 km broadens the group-path histogram, increasing the delay spread from 90.6 km to 240.8 km, while the shadow-zone width changes only moderately (164–172 km). This sensitivity arises because a larger acceptance window collects rays with more diverse paths, artificially inflating the apparent delay spread; accordingly, we adopted ±1 km as the primary criterion to balance stable ray collection with conservative multipath separation.

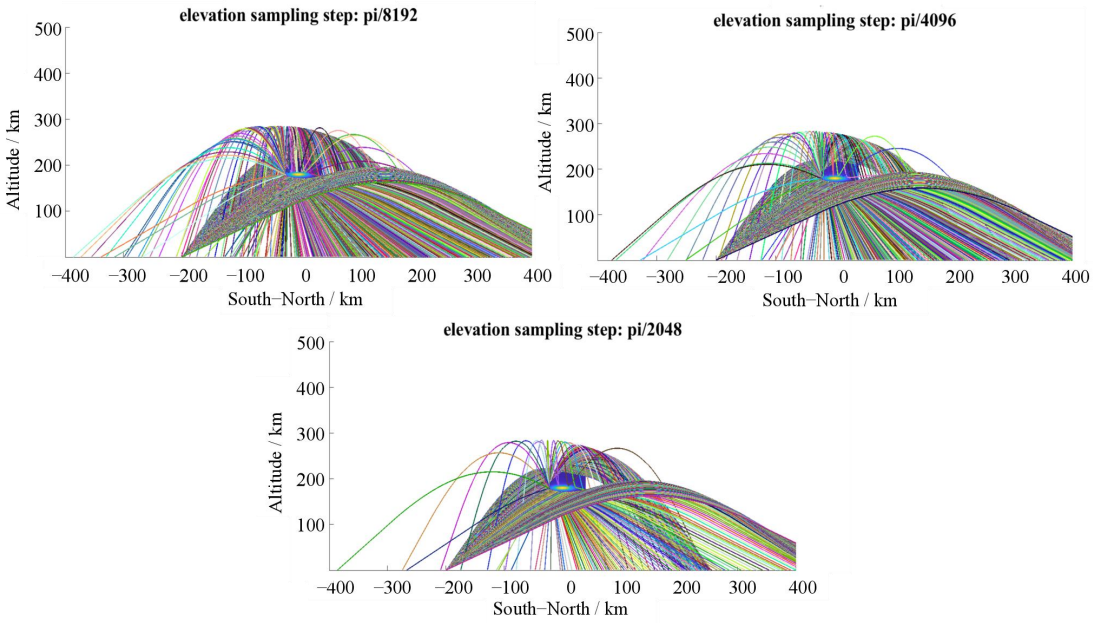


Figure S1. Ray-tracing results under different elevation sampling step

For the ray integration step, varying the step from 0.01 km to 0.10 km yields variations within 3% for both shadow and enhancement zone widths, confirming that 0.05 km provides a good balance between accuracy and computational cost. For the cloud evolution model, refining the spatial grid from 1 km to 0.5 km changes the peak electron density by only 2.8% (from 1.795×10^{13} to 1.745×10^{13} m^{-3}) and the cloud scale by 0.9%, while the shadow-zone width and enhancement-zone width vary by less than 4%. These small differences confirm that the baseline grid spacing of 1 km is adequate for capturing the cloud morphology and its propagation effects. The ray-tracing results under different ray integration step sizes (0.01 km; 0.05 km; 0.1 km) and different cloud spatial grid spacing (0.5 km; 1 km) were shown in Figure S2 and Figure S3 respectively. Overall, the sensitivity tests demonstrate that our main conclusions regarding the parameter-dependent trends are robust with respect to the numerical discretization and ray-tracing settings.

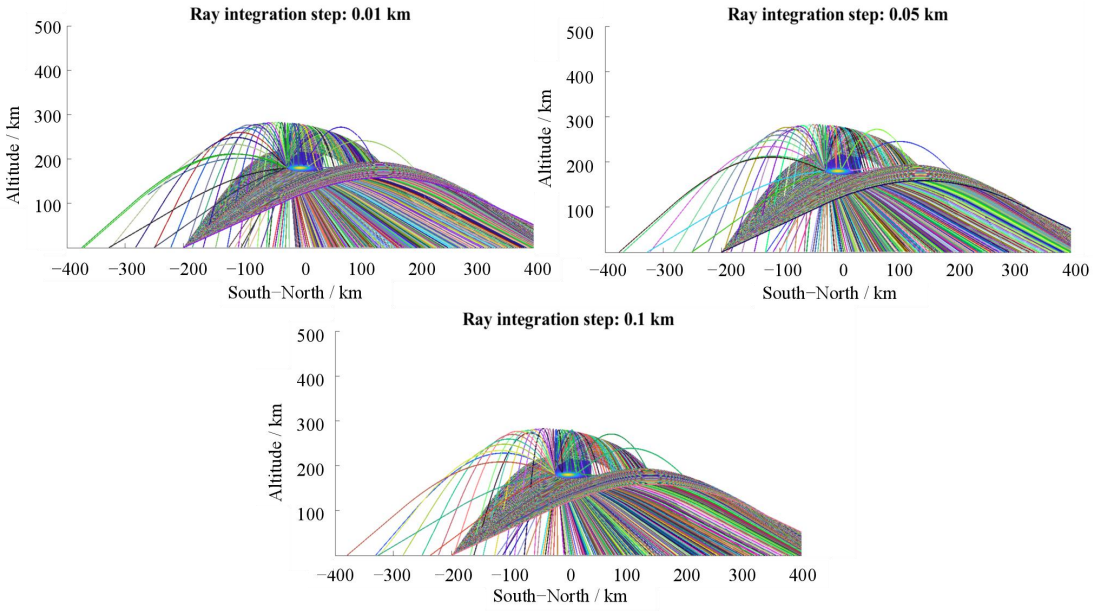


Figure S2. Ray-tracing results under different ray integration step sizes

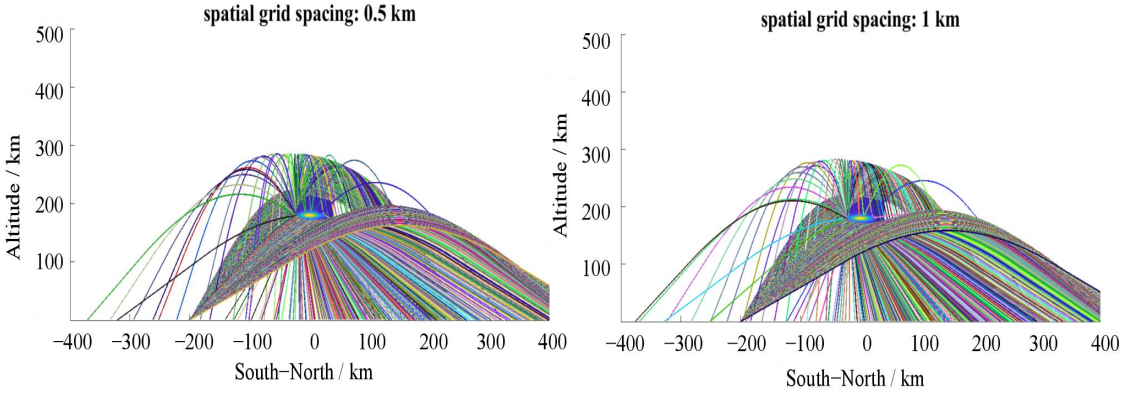


Figure S3. Ray-tracing results under different cloud spatial grid spacing